IEEE Access
Multidisciplinary ⋮ Rapid Review ⋮ Open Access Journal

Received 14 April 2024, accepted 25 May 2024, date of publication 1 July 2024, date of current version 9 July 2024.

Digital Object Identifier 10.1109/ACCESS.2024.3410394

RESEARCH ARTICLE

Transient Electromagnetic Signal Filtering Method Based on Intelligent Optimized Time–Space Fractional-Order Diffusion Equation

CHAO TAN[1,2], LINSHAN YU[1], JIWEI TAN[1], YAOHUI CHEN[1], CHANGJIANG HE[1], AND SHIBIN YUAN[1]

[1]College of Electrical and New Energy, China Three Gorges University, Yichang 443002, China
[2]Hubei Provincial Engineering Technology Research Center for Microgrid, China Three Gorges University, Yichang 443002, China

Corresponding author: Chao Tan (ctgutc@ctgu.edu.cn)

ABSTRACT To filter out noise in transient electromagnetic (TEM) signals, a Time-Space Fractional-order Diffusion Model (TSFDM) based on intelligent optimization is proposed. Firstly, based on the characteristics of the TEM signal, the signal is subjected to dynamic threshold segmentation processing. Then, the discrete difference method and the Grunwald-Letnikov approximation method with displacement are separately employed to approximate the time Caputo fractional derivative and the space Riemann-Liouville fractional derivative for solving the time-space fractional diffusion equation, this establishes an iterative convergent difference equation, and different smoothing operators corresponding to different stages of signal are set to obtain the TSFDM filter. Moreover, the Harris Hawk algorithm combined with Golden Sine and Energy-updating (GEHHO), is used to find the optimal value of the fitness function to obtain the optimal TSFDM filter for each stage signal. Simulation results show that after using the proposed method, the SNR of the TEM signal has increased by 33 dB, effectively restoring the trend of frequency domain curve changes. Compared to traditional methods, this approach demonstrates better performance in the evaluation metrics. Simulation experiments on geological structure inversion show that filtering and inversion of the noisy TEM signals yield results consistent with directly inverting the original signals.

INDEX TERMS Transient electromagnetic signal, intelligent optimization, segmentation, filter, time–space fractional-order diffusion equation.

I. INTRODUCTION

The Transient Electromagnetic (TEM) method is widely employed in resource exploration and geological research due to its advantages, such as remarkable exploration depth and exceptional resolution [1], [2]. However, the dynamic range of TEM signals is very large, and the amplitude decays as exponential curve. Especially for the late-stage signal, the Signal-to-Noise Ratio (SNR) of which is very low, and the signal is almost submerged by noise [3], [4].Therefore, signal preprocessing plays a pivotal role in the investigation of TEM, and attracts numerous scholars to study it. Therefore, signal preprocessing is a crucial link in the study of transient electromagnetic method, which has attracted many scholars to explore it in depth.

There are many filtering methods to deal with TEM signal, including Wavelet Transform (WT), Principal Component Analysis (PCA), Adaptive filtering method and Deep learning mechanism. Ji Yanju et al proposed an exponential fitting adaptive Kalman filter (EF-AKF) to remove mixed electromagnetic noise while protecting signal features [5]. whom utilized wavelet thresholding and stationary wavelet transforms to eliminate background noise and random spike noise in TEM signals respectively two years later [6];

The associate editor coordinating the review of this manuscript and approving it for publication was Mohamed Kheir.

Dai Xueping et al. employed discrete wavelet transform to separate the signal and noise in TEM signals. The principle is to conduct Fourier transform in the wavelet domain and retains the first eight detail coefficients for reconstruction, and for uncomplicated datasets, the curve-fitting techniques are additionally utilized to smooth out the signal. Research shows that the selection of wavelet basis has a vital impact on feature extraction and wavelet algorithm. Besides, wavelet algorithm is also limited by the number of decomposition levels [7]. Wu Xin et al. introduced the sampling function optimization method, which effectively improved the suppression ability of TEM signal power frequency noise through the bipolar synchronous sampling method. The attenuation characteristics of the filtered signal were not obvious enough [8]; Kass and Li established the PCA denoising method through data organization selection, covariance matrix construction, and principal component selection in reconstruction [9], which effectively removed the noise basis vector and preserve the effective signal. Feng Bing et al. used the Kernel Minimum Noise Fraction (KMNF) method to map data from the original space to the feature space through nonlinear mapping and then performed linear analysis on the data to extract nonlinear information from electromagnetic data. However, PCA and KMNF have strict data distribution assumptions and sensitivity to parameter selection, which lack flexibility in application [10]. On the basis, Lin Fangqiang et al. proposed the SFSDSA(secondary field signal denoising stacked autoencoders) model of deep neural network based on feature extraction and denoising. According to the depth characteristics of the signal, the noisy signal points are mapped to the high probability points of the clean signal as the reference to achieve the effect of signal denoising [11]. Luan H et al Luan H et al proposes a Singular Spectrum Analysis (SSA) for the grounded electrical source airborne transient electromagnetic (GREATEM) data de-noising. The window length was selected by particle swarm optimization algorithm, and then the data was decomposed and reconstructed by SSA algorithm, effectively improving the data quality [12]. The above methods have a great influence on the field of transient electromagnetic filtering. However, due to the complexity of precise signal extraction, the above methods have different degrees of limitations.

To solve the inherent limitations of the aforementioned methods, such as the constraints of Fourier transform and the difficulty of selecting basic functions, variational mode decomposition (VMD), empirical mode decomposition (EMD) and their improved algorithms are increasingly used in transient electromagnetic method signal processing in recent years. Wei Huiru et al. utilized the EMD to decompose TEM signals into multiple intrinsic mode functions ranging from high frequency to low frequency. Spectral analysis was performed on the intrinsic mode components, and effective signals were selected and reconstructed to obtain filtered signals. EMD has shortcomings such as modal aliasing and envelope fitting deviation. At the same time, the TEM signal was adaptively decomposed into different center frequency components through VMD, and the desired signal was reconstructed to achieve noise suppression, overcoming the difficulty of wavelet transform basis selection [13]; Feng et al. utilized the Whale Optimization Algorithm (WOA) to obtain the optimal penalty factor and decomposition level results in VMD, and then used the Bhattacharyya distance algorithm to identify effective patterns and noise patterns, achieving signal reconstruction [14]; Qi et al. utilized the Gray Wolf Algorithm (GWO) optimized VMD for adaptive decomposition of TEM signals, and then used wavelet thresholding to denoise the mixed-mode components and reconstruct the desired components to achieve TEM signal filtering [15].

The filtering effectiveness of the aforementioned methods is better than that of regular methods. However, the number of Intrinsic Mode Functions (IMFs) remains fixed when dealing with the entire time domain TEM signal. If the number is too large, it will bring early-stage signals to the endpoint effect; conversely, if the number is too small, it will reduce filtering effectiveness for later stage signals. Therefore, selecting a suitable number of IMFs is difficult. Whereupon, a segmented TEM filtering method for Time-Space Fractional Diffusion equations (TSFDM) was proposed. Among them, TSFDM is a diffusion model based on fractional order has long memory and good multiscale, which protects the signal features while flexibly dealing with the changes of different scales of the signal [16], and is suitable for dealing with nonlinear signals, therefore, it is attempted to apply TSFDM in the field of noise reduction of transient electromagnetic signals [17]. To obtain the optimal TSFDM filters for each stage signal, the improved Harris Hawk Optimization algorithm (GEHHO) is used for TSFDM optimization. The proposed method can effectively reduce the noise interference in the TEM signals while preserving the attenuation characteristics of the signals. Besides, The data quality and resolution of the inversion calculation are improved.

II. FILTERING MODEL AND IMPLEMENTATION STEPS

A. ALGORITHM FRAMEWORK

The filtering algorithm framework is shown in Fig. 1. Firstly, the TEM signal is converted into energy form, and energy dynamic thresholds are set to segment the signal. Next, the TSFDM and fitness function are established, meanwhile, the GEHHO is used to optimize the fitness function to obtain the optimal TSFDM filter for each stage signal. Then the overlapping averaging method is used to determine the concatenation points of filtered signals in each signal stage. Finally, a complete filtered TEM signal is obtained by splicing them together.

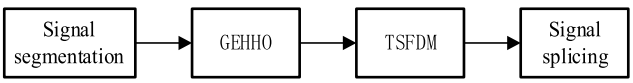

FIGURE 1. Filtering algorithm framework.

B. SEGMENTATION STRATEGY

The characteristics of TEM signal change with the increase of geological exploration depth: initially, the amplitude of voltage is high, during the transitional phase, it decays rapidly; it attenuates slowly and gradually tends to be smooth in the later stage. Therefore, TEM is segmented to obtain signals of different stages with different attenuation characteristics before filtering, and then the filtering model parameters and correlation functions corresponding to each segmented signal are adjusted to achieve better filtering results. According to the short-time energy variation law of transient electromagnetic signal, it is divided into three periods: early, middle and late. The specific segmentation process is as follows:

Set the TEM signal as $x(m)$, with N sampling points, which are processed by frame segmentation and windowing. Then, the short-time energy of each frame of the TEM signal by summing their squares. the short-time energy is defined as shown in equation (1) [18]:

$$\begin{cases} \omega(\mathrm{n}) = \begin{cases} 0.5(1-\cos(2\pi \mathrm{n}/(P-1))), 0 \le \mathrm{n} < P-1 \\ 0 \quad , \text{n=others} \end{cases} \\ E_{\mathrm{n}} = \sum_{\mathrm{m}=-\infty}^{\infty} [\mathrm{x}(\mathrm{m}) \times \omega(\mathrm{n}\text{-}\mathrm{m})]^2 \end{cases} \tag{1}$$

where $\omega(n)$ represents the Haining window function, Prepresents the window length. E_n represents the energy variation pattern of the TEM signal.

Set the energy dynamic thresholds as TH and TL, select the $E_n \ge TH$ period as the early stage of the signal, the $TH \ge E_n \ge TL$ period as the middle stage of the signal, and the $E_n \le TL$ period as the late stage of the signal. Each TEM stage signal extends N/1000 length before and after the breakpoint. The segmented signal is follows in equation (2):

$$\mathrm{S'}_i \begin{cases} \mathrm{S}_i(1), & 1 \le i \le X'(TH) + W \\ \mathrm{S}_i(2), & X'(TH) - W \le i \le X'(TL) + W \\ \mathrm{S}_i(3), & X'(TL) - W \le i \le N \end{cases} \tag{2}$$

where $\mathrm{S}_i(1)$, $\mathrm{S}_i(2)$, and $\mathrm{S}_i(3)$ are early, middle, and late stages signals respectively, $X'(TH)$ and $X'(TL)$ are the abscissa corresponding to the threshold of the TH and TL.

C. TIME-SPACE FRACTIONAL-ORDER DIFFUSED EQUATION FILTERING MODELING

The TSFDM is used to filter TEM signals from different stages. The proposed model exhibits a fractional-order memory property. Throughout the iterative filtering process, incorporating the prior signal information, the smoothing operator with the diffusion function is employed to weigh and update the gradient change results of both current and historical signals. As the increasing number of iterations, the smoothing operator suppresses the gradient value error caused by noise and preserves the signal characteristics effectively.

The TSFDM model employs the Caputo time fractional derivative of order a and the Riemann-Liouville space fractional derivative of order β to approximate the spatial and temporal derivatives in integer-order partial differential equations. This approach allows for obtaining the time-space fractional-order diffusion equation based on the classical diffusion model [19], as shown in equations. (3) and (4).

$$\frac{\partial^a u(x_i, t_k)}{\partial t^a} = G(u(x_i, t_k)) D_x^{\beta} u(x, t) \quad 1 < i < N, 0 < k \le L \tag{3}$$

$$u(x_i, t_0) = S_i(c) \, \mathrm{c} = 1, 2, 3 \tag{4}$$

where $a \in (0, 1)$, $\beta \in (1, 2)$, $\partial^a u(x_i, t_k) / \partial t^a$ is the Caputo fractional derivative of time order a; $D_x^{\beta} u(x_i, t_k)$ is the Riemann-Liouville fractional derivative of the space order β; S_{i} (c) is the segmented TEM signal to be filtered; N represents the number of sampling points of TEM signal; $u(x_i, t_k)$ represents the filtered signal obtained by k iterations of S_{i} (c), and x_i represents the i-th sampling point of the filtered signal in the space shift direction (the space displacement of the adjacent sampling points is h), $\mathrm{x}_i = ih$; t_k represents k iterations of the filtered signal in the time shift direction (time step $\tau = 1$), $t_k = k\tau$; and $G(u(x_{\mathrm{i}}, t_{\mathrm{k}}))$ is the Diffusion function, as shown in equation (5), which represent the diffusion coefficient corresponding to the i-th sample point of the sampling sequence after k iterations.

$$G(u(x_i, t_{k+1})) = \exp\left(-\left(\frac{|u(x_i, t_k)| \times \sqrt{-\ln(0.1)}}{\max[u(x_i, t_k) - \min u(x_i, t_k)]} \right)^2 \right) \tag{5}$$

To achieve the filtering discrete signals, a finite difference method is employed to discretize the continuous time-space fractional diffusion equation, transforming the problem of solving partial differential equations into solving algebraic equation systems. Therefore, the Caputo fractional derivative at the left end of the time-space fractional diffusion equation is approximated by difference discretization [20], while the Riemann Liouville fractional derivative at the right end of equation (4) is approximated by Grunwald-Letnikov with displacement [21], This approach allowed us to establish discrete difference equations of the TSFDM filters as follows:

$$U^0 = \left(A^0 + B^0\right)^{-1} U^0 \tag{6}$$

$$U^k = \left(A^{k-1} + B^{k-1}\right)^{-1} \left((1 - b_1) U^k + b_k U^0 + \sum_{j=1}^{k-1} (b_j - b_{j+1}) U^{k-j} \right) \tag{7}$$

where $b_j = (j+1)^{1-a} - j^{1-a}$, $U^n = \left[u_1^n, u_2^n, u_3^n, \cdots, u_N^n\right]$, u_i^k represents $u(x_i, t_k)$; equation (6) represents the first iteration filtering result of the input signal through the TSFDM filter; equation (7) represents the k iteration filtering result of the TSFDM filter; $(1 - b_1) U^k +$

$b_k U^0 + \sum_{j=1}^{k-1} \left(b_j - b_{j+1}\right) U^{k-j}$ represents the weighted of historical iteration results; The smoothing matrices A^k and $B^k$are shown in equations (8) and (9), shown at the bottom of the page; The time order is $a_i = |(u(x_i, t_1) - (u(x_i, t_2)| / (\max |(u(x_i, t_1) - (u(x_i, t_2)|)$. By subtracting the amplitude of each sampling point in the original signal from that of each sampling point in the first iteration filtered signal, a sequence of length N is obtained. In this sequence, the ratio between the difference value corresponding to each sampling point and the maximum difference value is used as the order for each sampling point, where $R_i^k = \tau^a \Gamma(2-a) G(u(x_i, t_k))/h^\beta$represents the weight factor of the smoothing matrix that contains diffusion functions.; The Grunwald-Letnikov approximation coefficient is $g_0 = 1, g_k = \left(1 - (\beta + 1/n)\right) g_{k-1}$; The smoothing coefficients K_1, K_2 are non-negative numbers, $K_1 + K_2 > 0$, and the matrix dimension$(M\text{-}1)$ is equal to the length of the signal.

Due to the voltage amplitude of TEM signal has different attenuation changes in various periods, when processing the early and middle stages signal, the coefficients K_1 and $K_2$for smoothing matrices A and B are set as column vectors, which are shown as equations (10) and (11), respectively. Among them, the elements in these vectors increase linearly, adjusting the weighting factor R_i in the smoothing matrix to adapt to the decreasing SNR during attenuation process, achieving a better smooth filtering effect. When processing the late-stage signal, the attenuation trend of the signal during this stage is relatively gentle, K_1 and K_2 are set as constant values of 50 and 0.1.

$$K_1 = \theta \left[1/(M-1), 2/(M-1) \cdots, (M-2)/(M-1), 1\right]_{1\times(M-1)}^{-1} \tag{10}$$

$$K_2 = \left[(\theta + \ln(M-1))^{-1}, (\theta + \ln(M-2))^{-1} \cdots, (\theta + \ln(1))^{-1}\right]_{1\times(M-1)}^{-1} \tag{11}$$

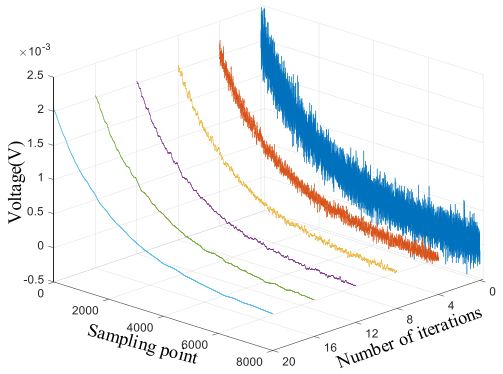

FIGURE 2. TSFDM iterative convergence diagram.

As shown in Fig.2, the diagram illustrates the convergence of TSFDM iterative filtering. As shown in Fig.2, is the filtering schematic of TSFDM iterative convergence. In this method, the random noise at each sampling point is suppressed continuously by the smoothing operator of weighted update during the 20 iterative filtering process of the noise added signal with the amplitude of the EMF decaying. Eventually, a signal curve with smooth attenuation characteristics is obtained, and the signal-to-noise ratio (SNR) is improved from 13 dB to 39 dB.

D. TSFDM PARAMETER OPTIMIZATION

1) FITNESS FUNCTION MODELING

In TSFDM filters, each stage signal corresponds to different space step sizes and space order values to achieve better filtering effects. Among them, the space step size represents the level of discretization in the spatial domain of the solution region. Appropriately reducing the value of space step size can improve spatial resolution. By dividing the solution domain into smaller intervals, more discrete spatial points can be obtained to capture smaller scale variations. The diffusion speed of the algorithm is also influenced by the space order. Furthermore, according to equations (8) and (9),

$$A^k = K_1 \begin{bmatrix} 1/K_1 - R_1^k g_1 - R_1^k g_2 & -R_1^k & & & & & \\ -R_2^k g_2 - R_2^k g_3 & 1/K_1 - R_2^k g_1 & -R_2^k & & & & \\ -R_3^k g_4 - R_3^k g_3 & -R_3^k g_1 & 1/K_1 - R_3^k g_1 & -R_3^k & & & \\ -R_4^k g_4 - R_4^k g_5 & -R_4^k g_3 & -R_4^k g_2 & 1/K_1 - R_4^k g_1 & -R_4^k & & \\ \cdots\cdots & \cdots\cdots & \cdots\cdots & \cdots\cdots & \cdots\cdots & & \\ -R_{M-2}^k g_{M-2} - R_{M-2}^k g_{M-1} & -R_{M-2}^k g_{M-3} & -R_{M-2}^k g_{M-4} & -R_{M-2}^n g_{M-4} & \cdots\cdots & -R_{M-2}^k & \\ -R_{M-1}^k g_{M-1} - R_{M-1}^k g_M & -R_{M-1}^k g_{M-2} & -R_{M-1}^k g_{M-3} & -R_{M-1}^n g_{M-4} & \cdots\cdots & 1/K_1 - R_{M-1}^k - R_{M-1}^k g_1 & \end{bmatrix}_{M-1\times M-1} \tag{8}$$

$$B^k = K_2 \begin{bmatrix} -R_1^k(1+g_1) & -R_1^k g_2 & -R_1^k g_3 & \cdots\cdots & -R_1^k g_{M-2} & -R_1^k(g_M + g_{M-1}) \\ -R_2^k & -R_2^k g_1 & -R_2^k g_2 & \cdots\cdots & -R_2^k g_{M-3} & -R_2^k(g_{M-1} + g_{M-2}) \\ & -R_3^k & -R_3^k g_1 & \cdots\cdots & -R_3^k g_{M-4} & -R_3^k(g_{M-2} + g_{M-3}) \\ & & \cdots\cdots & \cdots\cdots & \cdots\cdots & \cdots\cdots \\ & & & -R_{M-1}^k & -R_{M-1}^k g_1 & -R_{M-1}^k(g_2 + g_3) \\ & & & & -R_{M-1}^k & -R_{M-1}^k(g_1 + g_2) \end{bmatrix}_{M-1\times M-1} \tag{9}$$

the smoothing matrix weight factor R, which includes space step size and space order, has an impact on the filtering results. Therefore, when filtering processing segmented TEM signals with TSFDM, intelligent optimization algorithms are employed for parameter optimization to obtain the optimal TSFDM filter. The fitness function in the optimization algorithm is formulated as follows:

In the early and middle stages of the TEM signal, the amplitude of the voltage rapidly decays, and use the least squares method to obtain an estimated value that is similar to the attenuation characteristics of the signal. Then, the fitness function is set as the minimum absolute difference between the estimated $\varphi(x_i)$ value and U^3 (the filtering result calculated through two iterations of TSFDM with different parameter combinations). This minimum absolute difference corresponds to the optimal TSFDM filter.

$$\min_{\varphi} \sum_{i=1}^{m} |\delta_i| = \sum_{i=1}^{m} \left| \varphi(x_i) - U^3 \right| \tag{12}$$

The TEM signal decays slowly in the late stage, and the more orderly the arrangement of filtered data, the more pronounced the attenuation characteristics. Therefore, the lowest Permutation Entropy (PE) is used as the fitness function for this stage signal. By performing spatial reconstruction on the signal to obtain r components, arranging each reconstructed component in ascending order numerically, and obtaining a set of symbol sequences composed of column indices representing element positions, we can calculate the probabilities P_1, P_2, P_3, $\ldots P_n$ of occurrence for r different sequences. The time series permutation entropy is arranged according to equation (13), and the lowest permutation entropy corresponds to the optimal parameter combination of the TSFDM.

$$H = -\sum_{\mathrm{i}=1}^{\mathrm{r}} P_{\mathrm{i}} \ln P_{\mathrm{i}} \tag{13}$$

2) INTELLIGENT OPTIMIZATION ALGORITHM

The Improved Harris Hawk Optimization algorithm (GEHHO) is employed to optimize the fitness function to obtain the optimal TSFDM filter. Among them, GEHHO is based on the Harris Hawk (HHO) [22] algorithm, combining the golden sine function [23] and energy factor update strategy to enhance its global optimization performance. To traverse all numerical points within the range of space step size and space order as much as possible during the numerical search process. The specific process is as follows:

$$X\,(t+1) = \begin{cases} X_{rand}(t) - r_1\,|X_{rand}(t) - 2r_2X(t)| & q \geq 0.5 \\ (X_{rabbit}(t) - X_m(t)) - r_3\,(lb + r_4(ub - lb))\,, & q < 0.5 \end{cases} \tag{14}$$

From equation 14, Harris's hawk conducts random search when q≥0.5, without communicating with individuals in the population,which has resulted the algorithm's global search capability need to be improved, making it difficult to explore the whole solution space. Therefore, incorporating the Golden Sine function into the HHO exploration phase enhances its global search capability. The updated exploration formula is shown in equation (15):

$$X(t+1)\begin{cases} X(t)\,|\sin(R_1)| + R_2\sin(R_1) \times |x_1X_{rabbit} - x_2X(t)|\,, & q \geq 0.5 \\ (X_{rabbit}(t) - X_m(t)) - r_3\,(lb + r_4(ub - lb))\,, & q < 0.5 \end{cases} \tag{15}$$

where the golden section coefficients of x_1 and x_2 are:$x_1 = -\pi + (1-\gamma) \times 2\pi, x_2 = -\pi + \gamma \times 2\pi$, $R_1 \in [0, 2\pi]$, $R_2 \in [0, \pi]$, R_1determines the distance of individual movement in the next iteration, and R_2 determines the direction of individual position update in the next iteration. γ is golden section number, $\gamma = (\sqrt{5}-1)\big/2$.

As indicated by equation 16, the transition of Harris's hawk from global to local search is influenced by the escape energy factor E.

$$E = 2E_0(1 - \frac{\mathrm{t}}{T}) \tag{16}$$

where E_0 represents random number range of (−1,1), t represents the current number of iterations, and T represents the maximum number of iterations.

The energy factor E plays a balancing role between global search and local search. When $E < 1$, the algorithm performs local search, and when $E > 1$, the algorithm performs global exploration. From Fig.3, it can be observed that the energy factor of HHO becomes less than 1 after 220 iterations, indicating transition to local optimization. However, after 220 iterations, there is a probability that the energy factor formula (equation 17) in GEHHO becomes greater than 1, providing an opportunity to transition from local search back to global search.

$$E = 2E_0\frac{\mathrm{t}}{T}\mathrm{e}^{\left(-\frac{\mathrm{t}}{2T}\right)} + 2E_0\left(1 - \frac{\mathrm{t}}{T}\right) \tag{17}$$

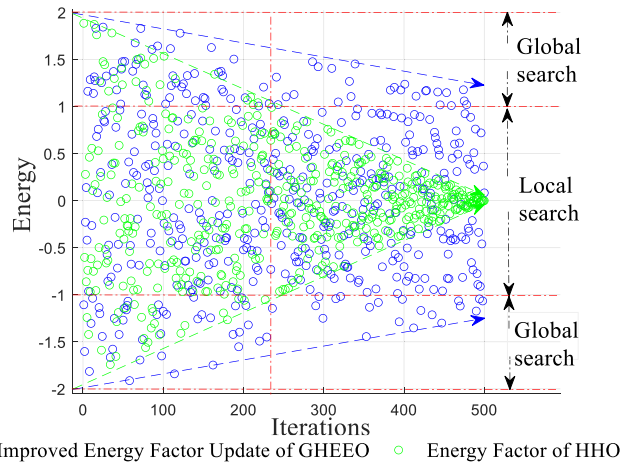

FIGURE 3. Energy factor.

E. SPLICING STRATEGY

As mentioned above, the transient electromagnetic signal is divided into three periods with the short-term energy variation law. After signal filtering, the signals originally split into three segments need to be concatenated again in series. If the splicing is improper, it may cause greater signal error. Therefore, the purpose of the splicing strategy is to make the filtering signals of the three periods be spliced with as little error as possible after filtering. The general idea is that three filtered signals output by GEHHO-TSFDM are concatenated in series to obtain the complete TEM filtered signal with the minimum error between the stitched points by the superposition average method. Firstly, the extended regions of the filtered signal in two adjacent stages are stacked, and calculate their average value. Then, this value is subtracted from the extended region of the next stage filtered signal, and take the absolute value, where the minimum value point is the splice point, as shown in equations (18).$U^k(1)$, $U^k(2)$ and $U^k(3)$ represent the filtered signals in the early, middle, and later stage respectively, I_1 min represents the splicing points of the early and middle stage filtered signal, whileI_2 min represents the splicing points of the middle and later stage filtered signal.

$$\begin{cases} I_1 \min = \left|((U^k(1) + U^k(2)))/2 - U^k(2)\right|, \\ X'(TH) - W \le i \le X'(TH) + W \\ I_2 \min = \left|((U^k(2) + U^k(3)))/2 - U^k(3)\right|, \\ X'(TL) - W \le i \le X'(TL) + W \end{cases} \tag{18}$$

Obtain the splice points I_1 min and I_2 min through equation (18), connect the adjacent filtered sequences from the splice points to obtain the complete filtered signal (U^k), as shown in equation (19).

After this strategy, the complete filtered TEM signal with minimum error is obtained.

$$U^k = \begin{cases} U^k(1), 1 \le i \le I_1 \min \\ U^k(2), I_1 \min \le i \le I_2 \min \\ U^k(3), I_2 \min \le i \le N \end{cases} \tag{19}$$

F. IMPLEMENTATION STEPS OF THE PROPOSED METHOD

The process of the GEHHO-TSFDM filtering diagram is shown in Fig.4. The steps are as follows:

Step 1: Calculate the short-term energy of the TEM signal and set the threshold to segment the signals. Select the fitness function corresponding to each signal stage.

Step 2: Initialize TSFDM parameters: set time order a, number of iterations, range of space step and space order, smoothing coefficients K_1, K_2.

Step 3: Calculate the smoothing matrix weighting factor R^0, the smoothing matrices A^0 and B^0. Next, from equation (6), the first iteration filtering result is obtained. and the a_1, R^k, A^k, B^k are updated. Next, the k iterations filtering result is obtained from equation (7).

Step 4: Initialize GEHHO parameters: population size and number of iterations.

Step 5: Repeat step 3 and input the filtered result of the two iterations with different parameters into the fitness function. GEHHO searches for the Minimum value of the fitness function to obtain the optimal parameters.

Step 6: Filter each stage of the signal using the optimal TSFDM filter and concatenate them to acquire a complete TEM signal.

III. SIMULATION TEST RESULTS

A. SIMULATION MODEL

Using MATLAB to generate the discrete time series shown in equation (20), its physical meaning is the time-domain TEM signals of three underground target bodies in the geological body space [24] and the theory TEM signal without noise is shown in Fig.5.

$$\begin{aligned} S(t) = {} & 2 \times 10^{-4} \exp(-t) + 6.5 \times 10^{-4} \exp(-9t) \\ & + 10^{-3} \exp(-17t) + 3.5 \times 10^{-6} + n(\mathrm{t}) \end{aligned} \tag{20}$$

where $n(t)$ represents the noise component, including Gaussian white noise, spike pulses, mixed sine wave noise. The noise amplitude can be adjusted to change the signal-to-noise ratio during simulation.

Filtering effect evaluation indicators: RMSE (Root Mean Square Error), SNR (Signal-to-Noise Ratio), MAPE (Mean Absolute Percentage Error).

$$RMSE = \sqrt{\frac{1}{N}\sum_{\mathrm{n}=0}^{N-1}(\mathrm{y}(\mathrm{n}) - \mathrm{s}(\mathrm{n}))^2} \tag{21}$$

$$SNR = 10\log\left(\sum_{\mathrm{i}=1}^{N}\mathrm{s}^2(i) \Big/ \sum_{\mathrm{i}=0}^{N-1}|\mathrm{y}(i) - \mathrm{s}(i)|^2\right) \tag{22}$$

$$MAPE = \frac{1}{N}\sum_{\mathrm{n}=1}^{N}\left|\frac{\mathrm{y}(i) - \mathrm{s}(i)}{\mathrm{s}(i)}\right| \times 100\% \tag{23}$$

s(n) and y(n) are the original signal and filtered signal, respectively.

B. FILTERING EFFICIENCY OF PROPOSED METHOD

Adding Gaussian white noise to the entire simulated TEM signal, simultaneously introducing spike pulse noise and mixed sine wave noise to the late stage of the signal, we obtained simulated TEM signals with 1 dB SNR. The signal consists of 20,000 sampling points, and the voltage amplitude decays exponentially from 0.18 mV to 3.5μV. The filtering process and conclusions are as follows:

1) Signal segmentation: The TEM signal is converted into short-time energy, and the energy threshold is set as 0.0467 and 0.0044, as shown in Fig. 6(a). Then extend 20 sampling points at the front and rear endpoints of each stage signal. Finally, the sampling point ranges of each stage TEM signal are: [1,100], [60,320], [280,20000].

2) GEHHO Optimization: The parameter optimization results of the GEHHO algorithm are shown in Fig.6(b).

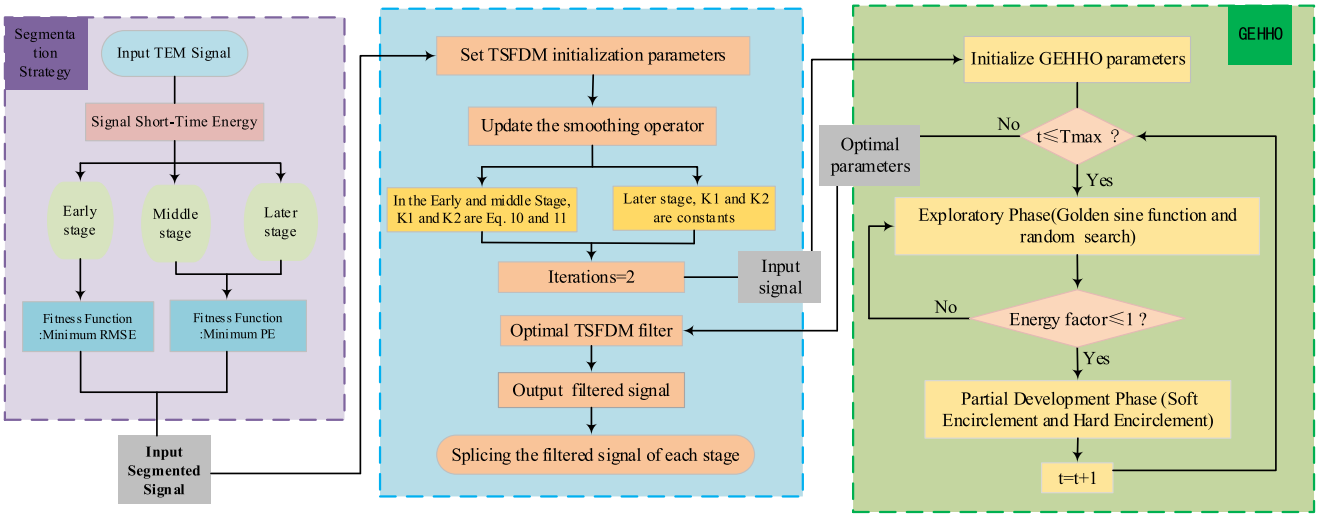

FIGURE 4. GEHHO-TSFDDM filter flowchart.

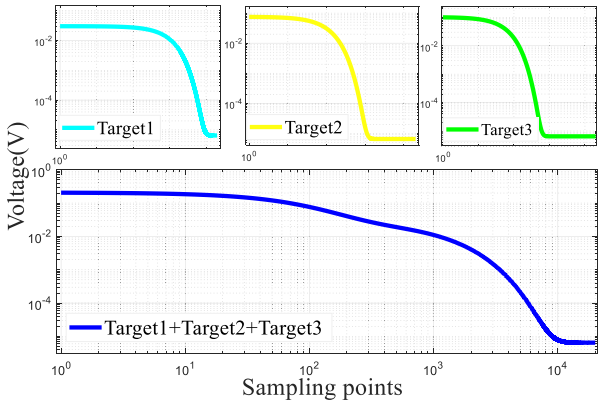

FIGURE 5. Multiple target theoretical TEM signal.

Compared with the HHO algorithm, the GEHHO algorithm achieves optimal values with fewer iterations than HHO. The parameter combinations for space order and space step are (1.50, 0.2384), (1.46, 0.0389), and (1.17, 0.0144) respectively.

3) Analysis of GEHHO-TSFDM filtering results: The filtered TEM signal with SNR of 34 dB is obtained by concatenating the output data of the optimal TSFDM filter, as shown in Fig.6(c). There are no endpoint effects or distortion phenomena during the early and middle stages of the signal. In the late stage, the filtered signal remains smooth and restores the attenuating characteristics of the original signal, Moreover, the RMSE decreases from $40.63 \times 10^{(-7)}$ to $0.85 \times 10^{(-7)}$, while the MAPE decreases from 91.45% to 1.64%. thus, verifying the feasibility of GEHHO-TSFDM.

C. COMPARISON SIMULATION

To validate the effectiveness of the proposed method, four models including VMD, EMD, Time Fractional Diffusion Model (TFDM) [25], and GEHHO-TSFDM are employed to filter TEM signals with different SNR of 1dB, -10dB, and -4dB. The types of noise included Gaussian white noise, impulse noise, and mixed sinusoidal waves. In the course of this process, VMD and EMD are used to filter the entire signal directly, maximizing improve the SNR of the TEM signal. Meanwhile, the TFDM adopted the same segmentation strategy as GEHHO-TSFDM and selected parameters through man-made experience. The following conclusions could be drawn from the analysis of the model output results:

TABLE 1. TEM signal filtering results with a SNR of 1.

	Noise signal	GEHHO-TSFDM	EMD	VMD	TFDM
SNR/dB	1	34	11	10	17
RMSE/$10^{(-7)}$	40.63	0.85	13.17	15.51	6.72
MAPE/%	91.45	1.64	28.54	19.28	14.33

TABLE 2. TEM signal filtering results with a SNR of −4dB.

	Noise signal	GEHHO-TSFDM	EMD	VMD	TFDM
SNR/dB	-4	30	5	8	11
RMSE/$10^{(-7)}$	88.40	1.43	25.99	18.98	13.03
MAPE/%	199.30	1.98	57.04	40.39	28.98

The evaluation results of the four models are shown in Table 1, Table 2 and Table 3. Among them, compared to the filtering results of the four models, GEHHO-TSFDM achieved the highest improvement in SNR, as well as the lowest MAPE and RMSE values. Compared with before filtering signals, the average MAPE and RMSE of the three filtered signals output by GHEOO-TSFDM decreased to

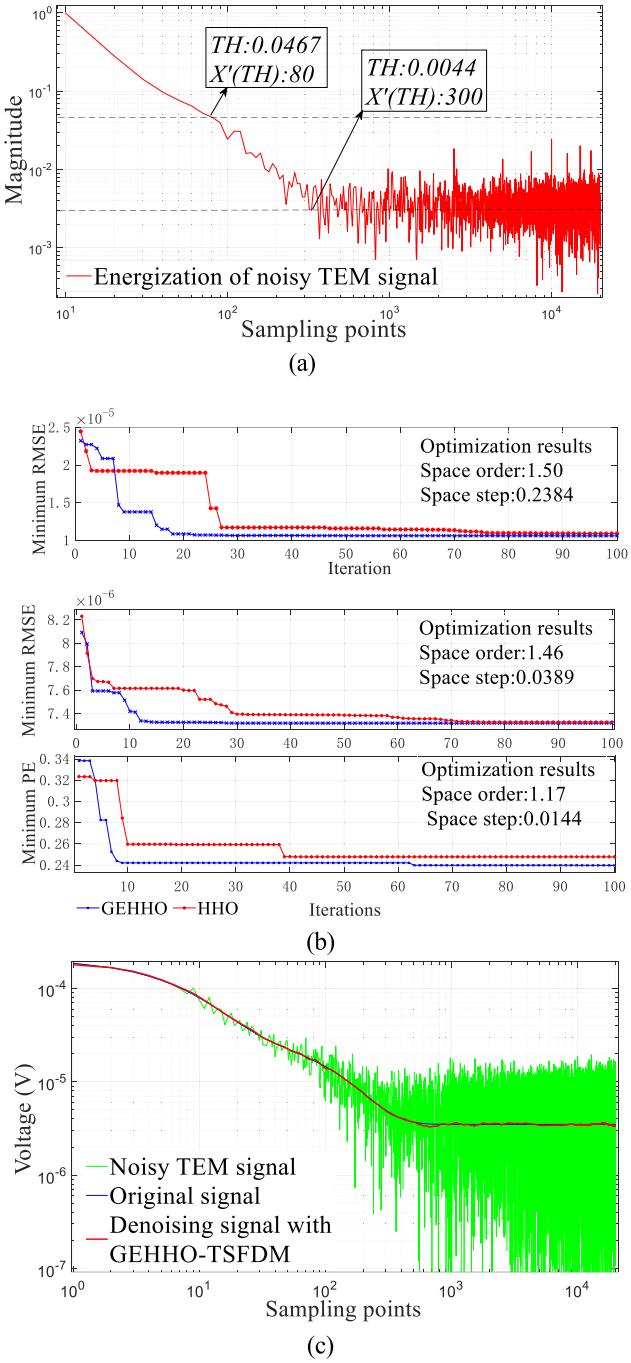

FIGURE 6. GEHHO-TSFDM filtering process and results; (a) Segmentation result (b) GEHHO optimization result (c) The filtered signal after GEHHO-TSFDM processing.

1.41% and 1.87%, respectively, while the average SNR increased by 33 dB.

The filtering effect diagram is shown in Fig.7(a). In the TEM signals filtered by VMD, EMD, and TFDM, there are many singular values in the middle stage of the signal, and the voltage amplitude fluctuates greatly in the late stage, which is not smooth enough. In addition, the filtered signal proceed by VMD exhibits endpoint effects in the early stage. The

TABLE 3. TEM signal filtering results with a SNR of −10dB.

	Noise signal	GEHHO-TSFDM	EMD	VMD	TFDM
SNR/dB	-10	24	1	4	9
RMSE/$10^{(-7)}$	157.62	3.02	24.96	21.96	17.63
MAPE/%	355.33	5.17	103.60	66.58	37.83

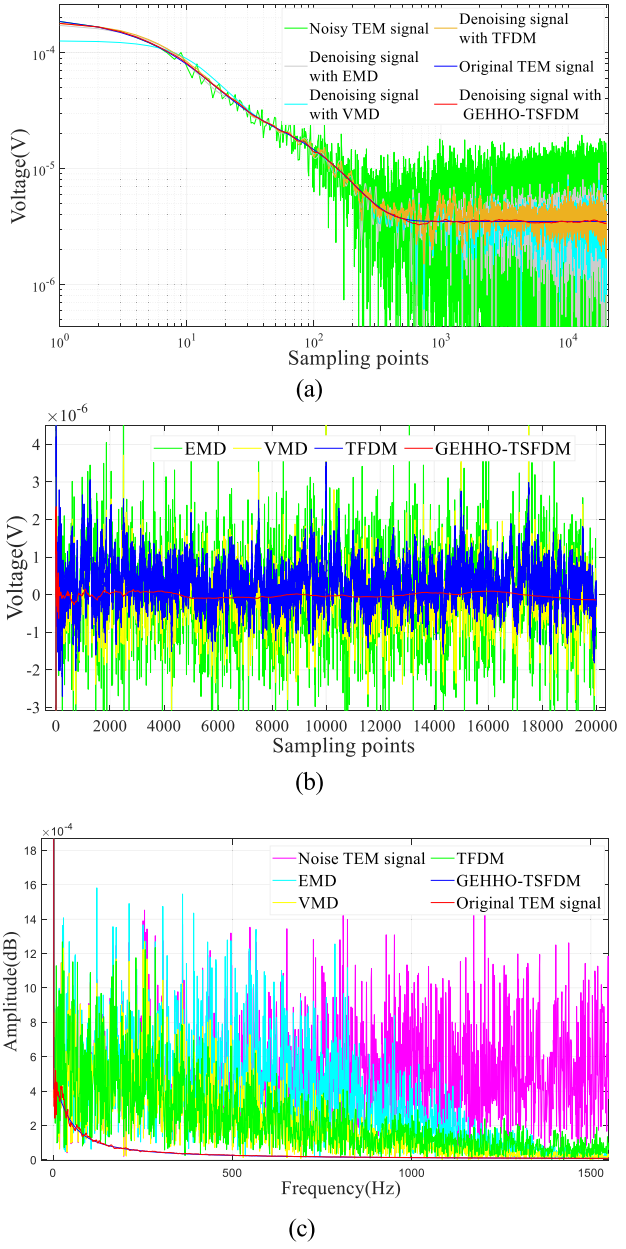

FIGURE 7. Comparison simulation result, (a) filtering results with different algorithms, (b) Comparison of absolute error curves, (c) Spectrum comparison chart.

error comparison between the filtered signal and the original signal, as shown in Fig.7(b), the GEHHO-TSFDM output signal has the smallest relative error, with a value of less than 1 μV, which indicates a higher degree of smoothness

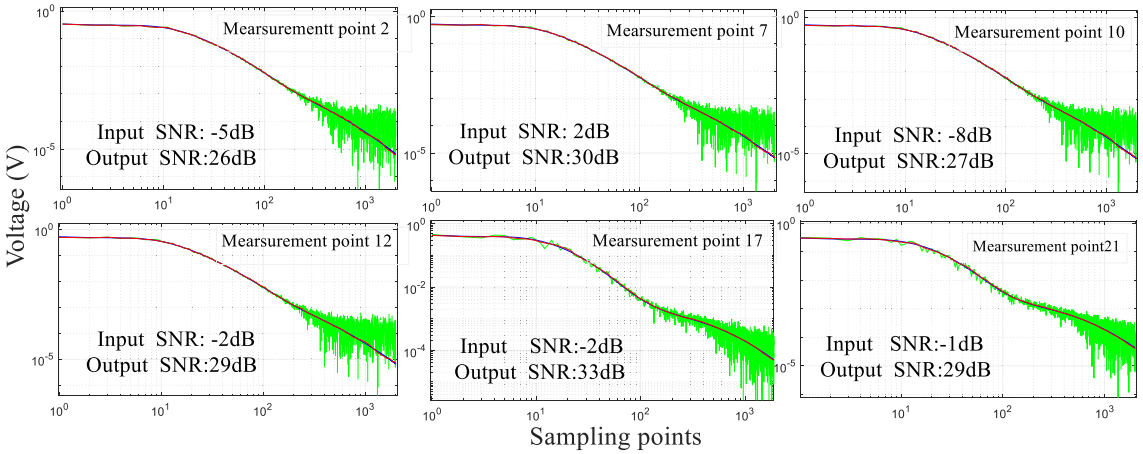

FIGURE 8. Filter results of transient electromagnetic signals at each measurement point.

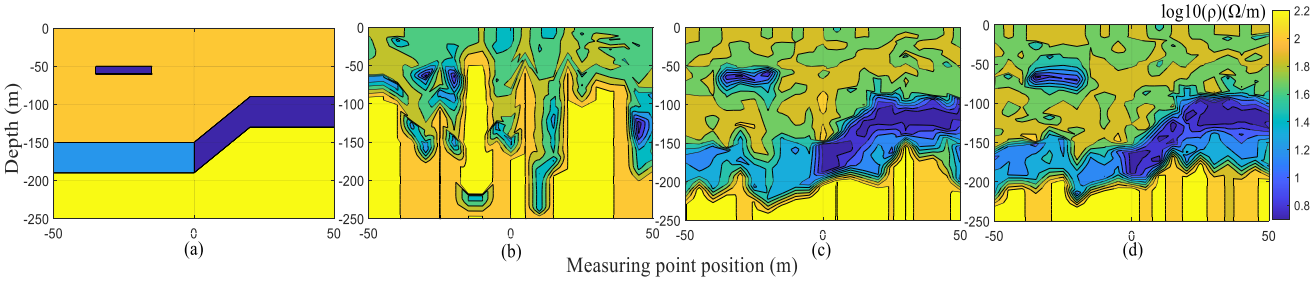

FIGURE 9. Comparison of inversion result before and after filtering (a) Simulated geoelectric structure diagram; (b) Inversion results of noisy data; (c) Inversion results of no-noise data; (d) Inversion results of filtered data.

in the signal. In the frequency spectrum of Fig.7(c), four models suppress noise above 1000Hz. However, the filtered signals of EMD, VMD, and TFDM exhibit significant fluctuations in the frequency curve within the range of 50Hz to 500Hz, whereas GEHHO-TSFDM effectively suppressed the abnormal protrusions in this frequency band and restored the attenuation trend of the original signal frequency domain curve.

The aforementioned analysis indicates that the proposed method exhibits capability in restoring the attenuation characteristics of TEM signals, with superior performance in various evaluation indicators results, indicating its effectiveness.

IV. EXPERIMENT AND DISCUSSION

In order to verify the feasibility of this method, comparing the inversion results of original signals, noisy signals and filtered signals.

1) Establish a standard geological body model diagram as shown in Fig.9(a). Then, 21 undisturbed measurement point TEM signals are generated in MATLAB and inverted to form a simulated geological body as shown in Fig.9(c), a low-resistance region with a resistance value of 5Ω·m and a length of 20 m is observed in the depth range of 50-70 m, and a layered low-resistance region with a resistance value of 5Ω·m is observed in the depth range of 150-190 m. In addition, stratified bands with resistance values of 20 Ω m exist at depths ranging from 90m to 180 m.

2) Then, Gaussian white noise is added to the entire undisturbed TEM signal of each measurement point, and spike pulse noise and mixed sine wave noise are added to the late-stage signals. This results in 21 noisy TEM signals with an average of -2dB. Inversion calculations are performed on these 21 noisy TEM signals, the results are shown in Fig.9(b), the geological information is fuzzy and incomplete, making it impossible to obtain effective geological information.

3) The GEHHO-TSFDM model is used to filter the noisy signal from 21 measuring points, resulting in a filtered signal with an average SNR of 28 dB. As shown in Fig.8, comparing original signals, noisy signals and filtered signals of measurement points 2, 7, 10, 12, 17, and 21, it can be seen that the original signal feature information is effectively reserved. Through the inversion imaging of the filtered signals, the geological structure is shown in Fig.9(d). Reproduces the layered resistance phenomenon depicted in Fig.9(c). The initial geological structure is effectively restored. This validates the feasibility of the proposed model.

V. CONCLUSION

To filter out noise and obtain TEM filtering signals with distinct decay characteristics, a segmented TEM filtering method based on GEHHO parameter optimization of the

Time-Space Fractional Diffusion equation is proposed. The method uses a segmented strategy and parameter-optimized TSFDM filtering model, which makes the model parameter values and function selection change adaptively with the signal characteristics of each stage in order to achieve a better filtering effect.

The simulation and experimental analysis results demonstrate an average improvement of approximately 33 dB in output SNR. Comparison between the signal before and after filtering, RMSE reduced by about 1.41%, and MAPE reduced by about 1.87%. High-frequency noise in TEM signals is effectively removed while low-frequency noise is suppressed. Compared to other filtering methods, such as VMD, EMD and TFDM, the superiority of TSFDM is verified. Furthermore, by filtering and inverting the measured signals, the results closely resemble the actual geological structure; thus, validating the effectiveness and feasibility and of this proposed method.

Certainly, the method still has some limitations. The proposed method uses the intelligent space-time fractional order equation, essentially uses a matrix to iterate the signal, and gets the filtered signal after several iterations. When the input electromagnetic signal is more complex, the order of the matrix is larger, the calculation speed will be greatly affected, and the filtering accuracy will also be reduced to a certain extent. On this basis, the calculation can be simplified by changing the size or sparsity of the matrix, so that the calculation speed can be maintained in complex cases, and this problem should be paid more attention in the follow-up research.

APPENDIX A

TSFDM employs the following time-space fractional nonlinear diffusion equation, as shown in (24):

$$\frac{\partial^a u(x_i,t_n)}{\partial t^a} = G\left(u(x_i,t_n)\right) D_x^\beta u(x_i,t_n) \quad 1 \le i \le N, 0 \le n \le L \tag{24}$$

where $\partial^a u(x_i,t_k)/\partial t^a$ represents the time Caputo fractional derivative, $D_x^\beta u(x_i,t_k)$ denotes the spatial Riemann-Liouville fractional derivative, $u(x_i,t_k)$ signifies the filtered signal obtained after n-1 iterations, N represents the number of sampling points in the input signal, L indicates the maximum iteration count, and $G(u(x_i,t_k))$ represents the diffusion function as shown in Equation (25).

$$G\left(u\left(x_i,t_n\right)\right) = \exp\left(-\left(\frac{|u(x_i,t_n)| \times \sqrt{-\ln(0.1)}}{\max\left[u\left(x_i,t_n\right) - \min u\left(x_i,t_n\right)\right]}\right)^2\right) \tag{25}$$

Firstly, the time fractional order is discretized directly, as shown in Equation (26):

$$\frac{\partial u^a(x_i,t_{n+1})}{\partial t^a} \approx \frac{\tau^{(-a)}}{\Gamma(2-a)} \sum_{j=0}^{n} b_j \left(u\left(x_i,t_{n+1-j}\right) - u\left(x_i,t_{n-j}\right)\right) \tag{26}$$

where the time order $a \in (0,1)$, $b_j^{(a)} = (j+1)^{1-a} - j^{1-a}$, $1 = b_1^{(a)} > b_2^{(a)} > \cdots > b_k^{(a)}$, τ represents the time step, indicating the time interval between adjacent temporal layers. $t_n = n\tau, n = 0, 1, \cdots, L$.

Then, for the space Riemann-Liouville fractional derivative, employ the displaced Grunwald-Letnikov approximation.

$$D_x^\beta u(x_i,t_{k+1}) \approx K_{10} D_x^\beta u(x_i,t_{k+1}) + K_{2x} D_N^\beta u(x_i,t_{k+1}) \tag{27}$$

where: ${}_0D_x^\beta u(x_i,t_{k+1}) = K_1 h^{-\beta} \sum_{j=0}^{i+1} g_j^{(\beta)} u\left(x_{i-j+1},t_{k+1}\right)$,

${}_xD_N^\beta u(x_i,t_{k+1}) = K_2 h^{-\beta} \sum_{j=0}^{M-i+1} g_j^{(\beta)} u\left(x_{i+j-1},t_{k+1}\right)$.

where K_1 and K_2 are non-negative constants, with the condition that $K_1 + K_2 > 0$. h is the space step size, which represents the distance between two sampling points (discrete interval). $x_i = ih, i = 0, 1, \cdots, N$; Space order $\beta \in (1,2)$; Grunwald-Letnikov approximation coefficients $g_0 = 1, g_j = \left(1 - (\beta+1)/j\right) g_{j-1}$, The time-space fractional diffusion equation difference format is established based on Equations (26) and (27), as shown in Equation (28):

$$\begin{aligned} &\frac{G\left(u(x_i,t_k)\right)^{(-1)} \tau^{(-a)}}{\Gamma(2-a)} \sum_{j=0}^{k} \left(u\left(x_i,t_{k+1-j}\right) - u\left(x_i,t_{k-j}\right)\right) \\ &= K_1 h^{-\beta} \sum_{j=0}^{i+1} g_j^{(\beta)} u\left(x_{i-j+1},t_{k+1}\right) \\ &\quad + \sum_{j=0}^{k} K_2 h^{-\beta} \sum_{j=0}^{M-i+1} g_j^{(\beta)} u\left(x_{i+j-1},t_{k+1}\right) \end{aligned} \tag{28}$$

Smooth matrix factor $R_i^k = \tau^a \Gamma(2-a) G\left(u(x_i,t_k)\right)/h^\beta$, $u(x_i,t_{k+1}) = u_i^{k+1}$.

When k=0:

$$\begin{aligned} &K_1 (R_{i+1}^0 u_{i+1}^1 + R_i^0 g_1 u_i^1 + R_{i-1^i}^0 g_2 u_{i-1}^1 + \sum_{j=3}^{i+1} R_{i-j+1}^0 g_j u_{i-j+1}^1) \\ &+ K_2 \left(R_i^0 u_i^1 + R_{i-1}^0 g_1 u_{i-1}^1 + R_{i+1}^0 g_2 u_{i+1}^1 \right. \\ &\left. + \sum_{j=3}^{M-i+1} R_{i+j-1}^0 g_j u_{i+j-1}^1 \right) = b_{(0)} (u_i^1 - u_i^0) \end{aligned} \tag{29}$$

Move u_i^1 to the left side of the equation and u_i^0 to the right side:

$$\begin{aligned} &K_1 (-R_{i+1}^0 u_{i+1}^1 - R_i^0 g_1 u_i^1 - R_{i-1}^0 g_2 u_{i-1}^1 \\ &\quad - \sum_{j=3}^{i+1} R_{i-j+1}^0 g_j u_{i-j+1}^1) + u_i^1 \\ &\quad + K_2 \left(-R_i^0 u_i^1 - R_{i-1}^0 g_1 u_{i-1}^1 - R_{i+1}^0 g_2 u_{i+1}^1 \right. \\ &\quad \left. - \sum_{j=3}^{M-i+1} R_{i+j-1}^0 g_j u_{i+j-1}^1 \right) = u_i^0 \end{aligned} \tag{30}$$

Merge similar items:

$$K_1(-R^0_{i+1}u^1_{i+1} - (R^0_i g_1 - \frac{1}{K_1})u^1_i - R^0_{i-1}g_2u^1_{i-1} - \sum_{j=3}^{i+1} R^0_{i-j+1}g_j u^1_{i-j+1}) + K_2\left(-R^0_i u^1_i - R^0_{i-1}g_1u^1_{i-1} - R^0_{i+1}g_2u^1_{i+1} - \sum_{j=3}^{M-i+1} R^0_{i+j-1}g_j u^1_{i+j-1}\right) = u^0_i \tag{31}$$

$$(A^0 + B^0)U^1 = U^0 \tag{32}$$

$$U^1 = \left[A^0 + B^0\right]^{-1} U^0 \tag{33}$$

where $U^1 = \left[u^1_1, u^1_2, u^1_3, \cdots, u^1_N\right]$,assume $u^0_0 = u^0_1, u^0_{M-1} = u^0_M$, A^0 and B^0 are smooth matrices, while $A^0_{i,j}$ and $B^0_{i,j}$ are elements of matrices A^0 and B^0.

$$A^0_{i,j} = \begin{cases} -R^0_i g_i - R^0_i g_{i+1}, & i = 1, j = 2, 3 \ldots M-1 \\ 1/K_1 - R^0_{M-1} - R^0_{M-1}g_1, & i = M-1, j = M-1 \\ 1/K_1 - R^0_i g_1, & i = j = 2, 3 \ldots M-2 \\ -R^0_i g_{i-j+1}, & j < i-1, i \neq 1, j \neq M-1 \\ -R^0_i, & j = i+1 \\ 0, & j > i+1 \end{cases} \tag{34}$$

$$B^0_{i,j} = \begin{cases} -R^0_1(1+g_1), & i = 1, j = 1 \\ -R^0_i(g_{M-i+1} + g_{M-i}), & i = 1, 2 \ldots M-1, j = M-1 \\ -R^0_i g_1, & i = j = 2, 3 \ldots M-2 \\ -R^0_i g_{j-i+1}, & j > i-1, i = j \neq 1, j \neq M-1 \\ -R^0_i, & i = j+1 \\ 0, & i > j+1 \end{cases} \tag{35}$$

Write it in the form of a matrix (36) and (37), shown at the bottom of the next page.

When k≥1:

$$u^{k+1}_i - u^k_i + \sum_{j=1}^{k} b_j\left(u^{k+1-j}_i - u^{k-j}_i\right) = K_2 \sum_{j=0}^{M-i+1} R^k_{i+j-1}g^{(\beta)}_j u^{k+1}_{i+j-1} + K_1\left(g^{(\beta)}_{(0)}R^k_{i+1}u^{k+1}_{i+1} + g^{(\beta)}_{(1)}R^k_i u^{k+1}_i + g^{(\beta)}_{(2)}R^k_{i-1}u^{k+1}_{i-1} + \sum_{j=3}^{i+1} R^k_{i-j+1}g^{(\beta)}_{(j)}u^{k+1}_{i-j+1}\right) \tag{38}$$

Move u^{k+1}_i to the right side of the Equation (38) and place u^k_i on the left side of the Eq. (38):

$$u^k_i - \sum_{j=1}^{k} b_j\left(u^{k+1-j}_i - u^{k-j}_i\right) = -K_2 \sum_{j=0}^{M-i+1} R^k_{i+j-1}g^{(\beta)}_j u^{k+1}_{i+j-1} - K_1\left(g^{(\beta)}_{(0)}R^k_{i+1}u^{k+1}_{i+1} + (g^{(\beta)}_{(1)}R^k_i - \frac{1}{K_1})u^{k+1}_i + g^{(\beta)}_{(2)}R^k_{i-1}u^{k+1}_{i-1} + \sum_{j=3}^{i+1} R^k_{i-j+1}g^{(\beta)}_{(j)}u^{k+1}_{i-j+1}\right) \tag{39}$$

Merge similar terms on the left side of Equation (39):

$$\begin{aligned} u^k_i - \sum_{j=1}^{k} b_j\left(u^{k+1-j}_i - u^{k-j}_i\right) &= u^k_i - \sum_{j=1}^{k} b_j u^{n+1-j}_i \\ &+ \sum_{j=1}^{k-1} b_j u^{k-j}_i + b_k u^0_i = u^n_i - \sum_{j=2}^{n} b_j u^{k+1-j}_i - b_1 u^k_i \\ &+ \sum_{j=1}^{k-1} b_j u^{k-j}_i + b_k u^0_i = u^k_i - \sum_{j=1}^{k-1} b_{j+1} u^{k+1-(j+1)}_i - b_1 u^k_i \\ &+ \sum_{j=1}^{k-1} b_j u^{k-j}_i + b_k u^0_i = (1-b_1)u^k_i + b_k u^0_i \\ &+ \sum_{j=1}^{k-1} (b_j - b_{j+1}) u^{k-j}_i \end{aligned} \tag{40}$$

Merge similar terms on the right side of Equation (39):

$$-K_1\left(g^{(\beta)}_{(0)}R^k_{i+1}u^{k+1}_{i+1} + (g^{(\beta)}_{(1)}R^k_i - \frac{1}{K_1})u^{k+1}_i + g^{(\beta)}_{(2)}R^k_{i-1}u^{k+1}_{i-1} + \sum_{j=3}^{i+1} R^k_{i-j+1}g^{(\beta)}_{(j)}u^{k+1}_{i-j+1}\right) - K_2 \sum_{j=0}^{M-i+1} R^k_{i+j-1}g^{(\beta)}_j u^{k+1}_{i+j-1} = \left[A^k + B^k\right] U^{k+1} \tag{41}$$

where $U^{k+1} = \left[u^{k+1}_1, u^{k+1}_2, u^{k+1}_3, \cdots, u^{k+1}_N\right]$, assume $u^k_0 = u^k_1, u^k_{M-1} = u^k_M$.

From Equation (40) and (41), it can be obtained that:

$$U^{k+1} = \left[A^k + B^k\right]^{-1} \times \left((1-b_1)U^k + b_k U^0 + \sum_{j=1}^{k-1}(b_j - b_{j+1})U^{k-j}\right) \tag{42}$$

where A^k and B^k are smooth matrices, while $A^k_{i,j}$ and $B^k_{i,j}$ are elements of matrices A^k and B^k.

$$A^k_{i,j} = \begin{cases} -R^k_i g_i - R^k_i g_{i+1}, & i=1, j=2,3\ldots M-1 \\ 1/K_1 - R^k_{M-1} - R^k_{M-1} g_1, & i=M-1, j=M-1 \\ 1/K_1 - R^k_i g_1, & i=j=2,3\ldots M-2 \\ -R^k_i g_{i-j+1}, & j<i-1, i\neq 1, j\neq M-1 \\ -R^k_i, & j=i+1 \\ 0, & j>i+1 \end{cases} \tag{43}$$

$$B^k_{i,j} = \begin{cases} -R^k_1(1+g_1), & i=1, j=1 \\ -R^k_i(g_{M-i+1}+g_{M-i}), & i=1,2\ldots M-1, j=M-1 \\ -R^k_i g_1, & i=j=2,3\ldots M-2 \\ -R^k_i g_{j-i+1}, & j>i-1, i=j\neq 1, j\neq M-1 \\ -R^k_i, & i=j+1 \\ 0, & i>j+1 \end{cases} \tag{44}$$

Equations (45) and (46), shown at the bottom of the next page. The order of A^k and B^k matrices: $M\text{-}1= N$

APPENDIX B

// TEM signals are converted to short-term energy
Set sampling frequency :Fs, frame length : wlen, frame shift:inc
win=hanning(wlen); // Generate Hanning window with length wlen
N=length(y); // Get the length N of the signal y
X=enframe(y,win,inc)';/ Split-frame the signal y with frame length wlen and frame shift inc to obtain the split-frame matrix X
fn=size(X,2);// Calculate the number of frames fn, i.e. the number of columns of the matrix X
time=(0:N-1)/Fs;// Calculate the time scale of the signal according to the sampling frequency Fs
for i=1: fn // For each frame (from 1 to fn)
u=X(:,i);// Take out frame i and store it in u
u2=u.*u;// Calculate the energy of the frame, i.e. the square of each sample, and store it in u2
En(i)=sum(u2);// The energies of a frame are summed up to get the total energy of the frame and stored in the En array
end
// TSFDM Implementation Steps
Input segmented signal, set the spatial step size h, spatial order p, temporal order *a*, diffusion threshold z, and iteration number gen
U(gen).ss=[];//Initialize U(gen).ss to an empty array.
F=max(U(1).ss-min(U(1).ss))./(-log(z)).^(0.5); // Calculate the diffusion coefficient for the first iteration
((1/(gen)).^a.*gamma(2-a))./h.^p; // Calculate the smoothing matrix weight factor
G(1)=-p; // Calculate the Grunwald-Letnikov approximation coefficients G
    for j=2:M
      G(j)=(1-(p+1)/j)*G(j-1);
    end
Set the values of K1 and K2, and if the signal is in the first or middle stages:
for i=1:M-1
    K1(i)=(10+log(i))^(-1);
end
for i=1:M
    K2(i)=30*(i/(M-1));
end
If the signal is late stage:
K1=50, K2=0.1;
Calculate the matrices A0 and B0 from Eqs. 8 and 9
The first iteration result U(2).ss is calculated from Eq. 6.
for j=2:gen //Set the number of iterations from 2 to gen
FF(j)=max(U(j).ss-min(U(j).ss))./((-log(z)).^(0.5));
// Updated diffusion coefficients

$$A^0 = K_1 \begin{bmatrix} 1/K_1 - R^0_1 g_1 - R^0_1 g_2 & -R^0_1 & & & & \\ -R^0_2 g_2 - R^0_2 g_3 & 1/K_1 - R^0_2 g_1 & -R^0_2 & & & \\ -R^0_3 g_3 - R^0_3 g_4 & -R^0_3 g_2 & 1/K_1 - R^0_3 g_1 & -R^0_3 & & \\ -R^0_4 g_4 - R^0_4 g_5 & -R^0_4 g_3 & -R^0_4 g_2 & 1/K_1 - R^0_4 g_1 & -R^0_4 & \\ \vdots & \vdots & \vdots & \vdots & \vdots & \\ -R^0_{M-2} g_{M-2} - R^0_{M-2} g_{M-1} & -R^0_{M-2} g_{M-3} & -R^0_{M-2} g_{M-4} & -R^0_{M-2} g_{M-4} & \cdots & -R^0_{M-2} \\ -R^0_{M-1} g_{M-1} - R^0_{M-1} g_M & -R^0_{M-1} g_{M-2} & -R^0_{M-1} g_{M-3} & -R^0_{M-1} g_{M-4} & \cdots & 1/K_1 - R^0_{M-1} - R^0_{M-1} g_1 \end{bmatrix}_{M-1\times M-1} \tag{36}$$

$$B^0 = K_2 \begin{bmatrix} -R^0_1(1+g_1) & -R^0_1 g_2 & -R^0_1 g_3 & \cdots & -R^0_1 g_{M-2} & -R^0_1(g_M + g_{M-1}) \\ -R^0_2 & -R^0_2 g_1 & -R^0_2 g_2 & \cdots & -R^0_2 g_{M-3} & -R^0_2(g_{M-1} + g_{M-2}) \\ & -R^0_3 & -R^0_3 g_1 & \cdots & -R^0_3 g_{M-4} & -R^0_3(g_{M-2} + g_{M-3}) \\ & & \ddots & \ddots & \ddots & \ddots \\ & & & -R^0_{M-1} & -R^0_{M-1} g_1 & -R^0_{M-1}(g_2 + g_3) \\ & & & & -R^0_{M-1} & -R^0_{M-1}(g_1 + g_2) \end{bmatrix}_{M-1\times M-1} \tag{37}$$

RR(j)=((1/(gen).^a.*gamma(2-a))./h.^p*exp(-(abs(U(j).ss)./FF).^2); // Update smoothing matrix weight factors
Updating the matrices Aj and Bj by Eqs. 8 and 9
for i=1:j-1// Update historical weighted results temp1 and temp2
if i==1
temp1=((i+1).^(1-a)-i.^(1-a)-(i+2).^(1-a)+(i+1).^(1-a)).*U(j-i).ss;
else
temp1=temp1+((i+1).^(1-a)-i.^(1-a)-(i+2).^(1-a)+(i+1).^(1-a)).*U(j-i).ss;
end
end
temp2=((j+1).^(1-a)-j.^(1-a)).*U(1).ss+(2-2.^(1-a)).*U(j).ss;
U(j+1).ss=(Q(j).ss)^(-1)*(temp1+temp2); // Calculate the filtered signal U(gen+1) from Equation (7).ss
end
//GEHHO Implementation steps
Setting the fitness function fobj, the dimension, the number of iterations T, the number of populations, the range of values of the parameters to be optimized lb and ub
t=0; //Loop counter
while t<T
for i=1:size(X,1) // Check boundries
FU=X(i,:)>ub;FL=X(i,:)<lb;X(i,:)=(X(i,:).*(~(FU+FL)))+ub.*FU+lb.*FL;
fitness=fobj(X(i,:)); // fitness of locations
if fitness<Rabbit_Energy // Update the location of Rabbit
Rabbit_Energy=fitness;
Rabbit_Location=X(i,:);
end
end
E1=2*exp(-0.5*(t/T));E0=(2*rand()-1)*(t/T);E2=2*(1-(t/T));
for i=1:size(X,1)
Escaping_Energy=E1*E0+E2*(2*rand()-1);
//escaping energy of rabbit
if abs(Escaping_Energy)>=1
// Exploration:Harris' hawks perch randomly based on 2 strategy:
q=rand();
if q>=0.5
r=rand();r1=(2*pi)*r;r2=r*pi;gold=double((sqrt(5-1)/2); // golden ratio
x1=-pi+2*pi*(1-gold); // Golden section coefficient x1
x2=-pi+2*pi*gold; // Golden section coefficient x2
X(i,:)=X(i,:)*abs(sin(r1))-r2.*sin(r1)*abs(x1*Rabbit_Location(1,:)-x2*X(i,:));
elseif q<0.5 %perch on a random tall tree (random site inside group's home range)
X(i,:)=(Rabbit_Location(1,:)-mean(X))-rand()*((ub-lb)*rand+lb);
end
elseif abs(Escaping_Energy)<1
// Exploitation:Attacking the rabbit using 4 strategies regarding the behavior of the rabbit
// phase 1: surprise pounce % surprise pounce: multiple, short rapid dives by different hawks
r=rand();
if r>=0.5 && abs(Escaping_Energy)<0.5 // Hard besiege
X(i,:)=(Rabbit_Location)-Escaping_Energy*abs(Rabbit_Location-X(i,:));
end
if r>=0.5 && abs(Escaping_Energy)>=0.5
// Soft besiege
Jump_strength=2*(1-rand()); // random jump strength of the rabbit
X(i,:)=(Rabbit_Location-X(i,:))-Escaping_Energy*abs(Jump_strength*Rabbit_Location-X(i,:));
end

$$A^k = K_1 \begin{bmatrix} 1/K_1 - R_1^k g_1 - R_1^k g_2 & -R_1^k & & & & & \\ -R_2^k g_2 - R_2^k g_3 & 1/K_1 - R_2^k g_1 & -R_2^k & & & & \\ -R_3^k g_3 - R_3^k g_4 & -R_3^k g_2 & 1/K_1 - R_3^k g_1 & -R_3^k & & & \\ -R_4^n g_4 - R_4^n g_5 & -R_4^k g_3 & -R_4^k g_2 & 1/K_1 - R_4^k g_1 & -R_4^k & & \\ \vdots & \vdots & \vdots & \vdots & \vdots & & \\ -R_{M-2}^k g_{M-2} - R_{M-2}^k g_{M-1} & -R_{M-2}^k g_{M-3} & -R_{M-2}^k g_{M-4} & -R_{M-2}^k g_{M-4} & \cdots & -R_{M-2}^k & \\ -R_{M-1}^k g_{M-1} - R_{M-1}^k g_M & -R_{M-1}^n g_{M-2} & -R_{M-1}^k g_{M-3} & -R_{M-1}^k g_{M-4} & \cdots & 1/K_1 - R_{M-1}^k - R_{M-1}^k g_1 & \end{bmatrix}_{M-1\times M-1} \tag{45}$$

$$B^k = K_2 \begin{bmatrix} -R_1^k(1+g_1) & -R_1^k g_2 & -R_1^k g_3 & \cdots & -R_1^k g_{M-2} & -R_1^k(g_M + g_{M-1}) \\ -R_2^k & -R_2^k g_1 & -R_2^k g_2 & \cdots & -R_2^k g_{M-3} & -R_2^k(g_{M-1} + g_{M-2}) \\ & -R_3^k & -R_3^k g_1 & \cdots & -R_3^k g_{M-4} & -R_3^k(g_{M-2} + g_{M-3}) \\ & & \ddots & \ddots & \ddots & \ddots \\ & & & -R_{M-1}^k & -R_{M-1}^k g_1 & -R_{M-1}^k(g_2 + g_3) \\ & & & & -R_{M-1}^k & -R_{M-1}^k(g_1 + g_2) \end{bmatrix}_{M-1\times M-1} \tag{46}$$

```
        if r<0.5 && abs(Escaping_Energy)>=0.5 // Soft besiege % rabbit try to escape by many zigzag deceptive motions
            Jump_strength=2*(1-rand());
X1=Rabbit_Location-Escaping_Energy*abs(Jump_strength *Rabbit_Location-X(i,:));
if fobj(X1)<fobj(X(i,:)) // improved move
    X(i,:)=X1;
else // hawks perform levy-based short rapid dives around the rabbit
X2=Rabbit_Location-Escaping_Energy*abs(Jump_strength *Rabbit_Location-X(i,:))+rand(1,dim).*Levy(dim);
            if (fobj(X2)<fobj(X(i,:))) // improved move
               X(i,:)=X2;
            end
        end
    end
if r<0.5 && abs(Escaping_Energy)<0.5 // Hard besiege rabbit try to escape by many zigzag deceptive motions
    // hawks try to decrease their average location with the rabbit
        Jump_strength=2*(1-rand());
        X1=Rabbit_Location-Escaping_Energy*abs
        (Jump_strength*Rabbit_Location-mean(X));
        if fobj(X1)<fobj(X(i,:)) // improved move
           X(i,:)=X1;
        else // Perform levy-based short rapid dives around the
        rabbit
X2=Rabbit_Location-Escaping_Energy*abs(Jump_strength *Rabbit_Location-mean(X))+rand(1,dim).*Levy(dim);
    if (fobj(X2)<fobj(X(i,:))) // improved move
       X(i,:)=X2;end;end;end;end;end
          t=t+1;
    end; end
function O=Levy(d) // Levy flight strategy
beta=1.5;
sigma=(gamma(1+beta)*sin(pi*beta/2)/(gamma((1+beta)/2) *beta*2^((beta-1)/2)))^(1/beta);
u=randn(1,d)*sigma;v=randn(1,d);step=u./abs(v).^(1/beta);
O=step;
end
```

REFERENCES

[1] Q. Y. Di, "New development of the electromagnetic (EM) methods for deep exploration," *J. Geophys.*, vol. 62, no. 6, pp. 2128–2138, 2019, doi: 10.6038/cjg2019M0633.

[2] L. Zhang, L. Xu, Y. Xiao, and N. Zhang, "Application of comprehensive geophysical prospecting method in water accumulation exploration of multilayer goaf in integrated mine," *Adv. Civil Eng.*, vol. 2021, pp. 1–12, Sep. 2021, doi: 10.1155/2021/1434893.

[3] Y. Su and X. Song, "Analysis of response characteristics of ground-well transient electromagnetic method," in *Proc. 4th Int. Conf. Intell. Control, Meas. Signal Process. (ICMSP)*, Hangzhou, China, Jul. 2022, pp. 5–8.

[4] S. Rasmussen, N. S. Nyboe, S. Mai, and J. Juul Larsen, "Extraction and use of noise models from transient electromagnetic data," *Geophysics*, vol. 83, no. 1, pp. E37–E46, Jan. 2018, doi: 10.1190/geo2017-0299.1.

[5] Y. Ji, Q. Wu, Y. Wang, J. Lin, D. Li, S. Du, S. Yu, and S. Guan, "Noise reduction of grounded electrical source airborne transient electromagnetic data using an exponential fitting-adaptive Kalman filter," *Explor. Geophys.*, vol. 49, no. 3, pp. 243–252, Jun. 2018, doi: 10.1071/eg16046.

[6] Y. Ji, D. Li, G. Yuan, J. Lin, S. Du, L. Xie, and Y. Wang, "Noise reduction of time domain electromagnetic data: Application of a combined wavelet denoising method," *Radio Sci.*, vol. 51, no. 6, pp. 680–689, Jun. 2016, doi: 10.1002/2016RS005985.

[7] X. Dai, L. Z. Cheng, J.-C. Mareschal, D. Lemire, and C. Liu, "New method for denoising borehole transient electromagnetic data with discrete wavelet transform," *J. Appl. Geophys.*, vol. 168, pp. 41–48, Sep. 2019, doi: 10.1016/j.jappgeo.2019.05.009.

[8] X. Wu, "Noise reduction technology by transient electromagnetic sampling function optimization," *Chin. J. Geophys.*, vol. 60, no. 9, pp. 3677–3684, 2017, doi: 10.6038/cjg20170931.

[9] M. A. Kass and Y. Li, "Quantitative analysis and interpretation of transient electromagnetic data via principal component analysis," *IEEE Trans. Geosci. Remote Sens.*, vol. 50, no. 5, pp. 1910–1918, May 2012, doi: 10.1109/TGRS.2011.2167978.

[10] B. Feng, J.-F. Zhang, P.-J. Gao, J. Li, and Y. Bai, "Nonlinear noise reduction for the airborne transient electromagnetic method based on kernel minimum noise fraction," *J. Environ. Eng. Geophys.*, vol. 26, no. 2, pp. 165–175, Jun. 2021, doi: 10.32389/jeeg20-020.

[11] F. Lin, K. Chen, X. Wang, H. Cao, D. Chen, and F. Chen, "Denoising stacked autoencoders for transient electromagnetic signal denoising," *Nonlinear Processes Geophys.*, vol. 26, no. 1, pp. 13–23, Mar. 2019, doi: 10.5194/npg-26-13-2019.

[12] H. Luan, X. Yu, Y. Wang, Q. Wu, and B. Tian, "Research on de-noising method of grounded electrical source airborne transient electromagnetic data based on singular spectrum analysis," *Appl. Sci.*, vol. 12, no. 19, p. 10116, Oct. 2022, doi: 10.3390/app121910116.

[13] H. Wei, T. Qi, G. Feng, and H. Jiang, "Comparative research on noise reduction of transient electromagnetic signals based on empirical mode decomposition and variational mode decomposition," *Radio Sci.*, vol. 56, no. 10, pp. 1–19, Oct. 2021, doi: 10.1029/2020RS007135.

[14] G. Feng, H. Wei, T. Qi, X. Pei, and H. Wang, "A transient electromagnetic signal denoising method based on an improved variational mode decomposition algorithm," *Measurement*, vol. 184, Nov. 2021, Art. no. 109815, doi: 10.1016/j.measurement.2021.109815.

[15] T. Qi, X. Wei, G. Feng, F. Zhang, D. Zhao, and J. Guo, "A method for reducing transient electromagnetic noise: Combination of variational mode decomposition and wavelet denoising algorithm," *Measurement*, vol. 198, Jul. 2022, Art. no. 111420, doi: 10.1016/j.measurement.2022.111420.

[16] A. Ben-Loghfyry and A. Hakim, "Robust time-fractional diffusion filtering for noise removal," *Math. Methods Appl. Sci.*, vol. 45, no. 16, pp. 9719–9735, Nov. 2022, doi: 10.1002/mma.8331.

[17] Y. Li, "Signal smoothing with time-space fractional order model," *Meas. Sci. Rev.*, vol. 21, no. 1, pp. 25–32, Feb. 2021, doi: 10.2478/msr-2021-0004.

[18] H. B. Lin, Y. Li, and X.C. Xu, "Segmenting time-frequency peak filtering method to attenuation of seismic random noise," *Chin. J. Geophys.*, vol. 54, no. 5, pp. 1358–1366, 2011, doi: 10.3969/j.issn.0001-5733.2011.05.025.

[19] P. Perona and J. Malik, "Scale-space and edge detection using anisotropic diffusion," *IEEE Trans. Pattern Anal. Mach. Intell.*, vol. 12, no. 7, pp. 629–639, Jul. 1990, doi: 10.1109/34.56205.

[20] T. Wei, "Implicit difference approximation of fractional time-space diffusion equation," *J. Lanzhou Univ. Arts Sci. Natural Sci. Ed.*, vol. 31, no. 6, pp. 21–24. 2017.

[21] Z. Z. Sun and G. H. Gao, Eds. *Finite Difference Methods for Fractional Differential Equations*, 11st ed. Beijing, China: Science Press, 2015, pp. 129–138.

[22] A. A. Heidari, S. Mirjalili, H. Faris, I. Aljarah, M. Mafarja, and H. Chen, "Harris hawks optimization: Algorithm and applications," *Future Gener. Comput. Syst.*, vol. 97, pp. 849–872, Aug. 2019, doi: 10.1016/j.future.2019.02.028.

[23] J. Xie, S. Huang, D. Wei, and Z. Zhang, "Scheduling of multisensor for UAV cluster based on Harris hawks optimization with an adaptive golden sine search mechanism," *IEEE Sensors J.*, vol. 22, no. 10, pp. 9621–9635, May 2022, doi: 10.1109/JSEN.2022.3164018.

[24] K. Chen et al., "TEMDnet: A novel deep denoising network for transient electromagnetic signal with signal-to-image transformation," *IEEE Trans. Geosci. Remote Sens.*, 2020, doi: 10.1109/TGRS.2020.3034752.
[25] Y. Li, Y. Ding, and T. Li, "Nonlinear diffusion filtering for peak-preserving smoothing of a spectrum signal," *Chemometric Intell. Lab. Syst.*, vol. 156, pp. 157–165, Aug. 2016, doi: 10.1016/j.chemolab.2016.06.007.

CHAO TAN received the B.S. and M.S. degrees in measurement control technology and instruments and the Ph.D. degree in geological resources and geological engineering from China University of Geosciences, Wuhan, China, in 2005, 2008, and 2011, respectively. He is currently an Associate Professor with the College of Electrical Engineering and New Energy, China Three Gorges University. His research interests include weak magnetic sensor, weak magnetic-field measurement method and instrumentation, and weak signal detection and process.

LINSHAN YU received the B.S. degree from the College of Computer Science and Technology, China Three Gorges University, Yichang, China. She is currently pursuing the M.S. degree in electrical engineering with China Three Gorges University. Her research interest includes signal processing.

JIWEI TAN received the B.S. degree in electrical engineering and automation from the Hao Ging College, Shaanxi University of Science and Technology. He is currently pursuing the M.S. degree in electrical engineering with China Three Gorges University, Yichang, China. His research interest includes signal processing.

YAOHUI CHEN received the B.S. degree from the College of Electrical and Electronic Information, Nanchang Hangkong University, Nanchang, China, in 2023. He is currently pursuing the M.S. degree in control science and engineering with China Three Gorges University, Yichang, China. His research interest includes biological magnetic field.

CHANGJIANG HE received the B.S. degree in electrical engineering and automation from the College of Electrical Engineering, Henan Polytechnic University of Technology, Jiaozuo, China, in 2023. He is currently pursuing the M.S. degree in electrical engineering with China Three Gorges University, Yichang, China. His research interest includes load forecasting.

SHIBIN YUAN received the B.S. degree in electrical engineering and automation from Guangling College of Yangzhou University. He is currently pursuing the M.S. degree in control engineering with China Three Gorges University, Yichang, China. His research interest includes power electronics.